NASA Technical Memorandum 82678

Application of "Steady" State Finite Element and Transient Finite Difference Theory to Sound Propagation in a Variable Area Duct: A Comparison with Experiment

Kenneth J. Baumeister
Lewis Research Center
Cleveland, Ohio

and

W. Eversman and R. J. Astley
University of Missouri
Rolla, Missouri

and

J. W. White
University of Tennessee
Knoxville, Tennessee

Prepared for the
Seventh Aeroacoustics Conference
sponsored by the American Institute of Aeronautics and Astronautics
Palo Alto, California, October 5-7, 1981

NASA

APPLICATION OF "STEADY" STATE FINITE ELEMENT AND TRANSIENT FINITE DIFFERENCE THEORY TO SOUND PROPAGATION IN A VARIABLE DUCT: A COMPARISON WITH EXPERIMENT

Kenneth J. Baumeister
National Aeronautics and Space Administration
Lewis Research Center
Cleveland, Ohio

W. Eversman and R. J. Astley
University of Missouri
Rolla, Missouri

and

J. W. White
University of Tennessee
Knoxville, Tennessee

E-960

Abstract

Sound propagation without flow in a rectangular duct with a converging-diverging area variation is studied experimentally and theoretically. The area variation was of sufficient magnitude to produce large reflections and induce modal scattering. The rms (root-mean-squared) pressure and phase angle on both the flat and curved surface were measured and tabulated. The "steady" state finite element theory of Astley and Eversman and the transient finite difference theory of White are in good agreement with the data. It is concluded that numerical finite difference and finite element theories appear ideally suited for handling duct propagation problems which encounter large area variations.

List of Symbols

c_0^*	speed of sound, m/s
f^*	frequency, Hz
h^*	duct height ahead of area change, m
H^*	maximum height of area change, m
J	function of x and y, Ref. 12
k	dimensionless reduced frequency, $\omega^* h^*/c_0^*$
L^*	length of area variation, m
P	time dependent dimensionless pressure, $P^*(x^*,y^*,t^*)/\rho_0^* c_0^{*2}$
p	Fourier transform pressure, $p^*(x,y)/\rho_0^* c_0^{*2}$
p_0	mean pressure, $p_0^*(x,y)/\rho_0^* c_0^{*2}$
S	standing wave ratio
t	dimensionless time, $t^* f^*$
U_0	mean axial velocity, U_0^*/c_0^*
u	acoustic axial velocity, u^*/c_0^*
V_0	mean transverse velocity, V_0^*/c_0^*
v	acoustic transverse velocity, v^*/c_0^*
x	dimensionless axial coordinate, x^*/h^*
y	dimensionless transverse coordinate, y^*/h^*
Y'	height of area variation, Eq. (1)
Z_e	exit acoustic impedance, $kg/m^2 sec$
α_r	sound power reflection coefficient, Eq. (10)
$\alpha, \beta, \gamma_1, \sigma, \tau$	function of x and y, Ref. 12
γ	specific heat ratio
η	transverse coordinate in transformed plane, see Fig. 5
ξ	axial coordinate in transformed plane, see Fig. 5
ρ_0^*	reference density, kg/m^3
ω	dimensionless frequency $h^* f^*/c_0^*$
ω^*	angular frequency, rad/sec

Superscript:

*	dimensionless quantity

Introduction

"Steady" state and transient finite difference and finite element theories have been developed to study sound propagation in complex ducts with axial variations in cross-sectional area, wall liner impedance (absorbers) and with gradients in flow Mach number. Reference 1 contains a comprehensive description of the techniques, advantages, and limitations associated with the various numerical solutions of the sound propagation equations. In general, the literature is concerned primarily with theoretical solutions of the sound propagation equations. The present paper concentrates on the experimental verification of the numerical theories particularly for ducts with large area variations.

Only a limited number of experimental studies is available to verify the numerical as well as the analytical sound propagation theories. For straight soft wall ducts, measured transmission

losses and axial pressure variations are in reasonable agreement with analytical[2,3] and finite element[4] theories. For acoustic filters and mufflers with abrupt area changes, finite element predictions of transmission losses[5,6] are also in good agreement with theory. Kagawa, et al.[7] recently developed a combination of the finite element (in duct) and analytical methods (Greens-Theorem in the far field) to analyze sound propagation from a loud speaker. The measured far field sound pressure and directivity characteristics were predicted within a few decibels over a wide frequency range. In a much simpler approach, Ref. 8 relates in duct finite element solutions to trends in the radiated far field data.

Nayfeh, et al.[9,10] experimentally studied sound propagation in an annular duct with a centerbody with a slowly varying cross sectional area. This experimental test section was designed to comply with the assumption inherent in their multiple scale perturbation analysis. The centerbody slope was limited to 0.2 to reduce reflections and coupling among acoustic modes, both of which are neglected in the analysis. The circumferential variations of pressure amplitude and phase at several axial positions were examined with hard walls and lined sections with and without mean flow. Reasonable agreement between the theoretical and experimental results were found for the converging portions of the duct.

The present study involves a similar experiment with axial area variations but ... hard wall rectangular duct with no flow. In contrast to Refs. 9 and 10, however, large slopes in the duct wall will be introduced to enhance reflections and modal scattering to obtain a severe test of the theory. Also axial pressure measurements are made in both the converging and diverging portion of the duct.

In the present paper, the experimental test section, apparatus and procedure will first be discussed. The experimental data will be conveniently tabulated for later use in the literature. Then, one steady state finite element theory[11] and one transient finite difference theory[12] will be compared to the data and conclusions drawn.

Experimental Apparatus and Procedure

To verify the numerical theories for hard walls without mean flow, the general acoustic duct system described in[13] was modified into the simple no flow apparatus shown in Fig. 1. The system shown in Fig. 1 was adapted to simulate plane wave propagation in an infinite duct. The following paragraphs describe the acoustic system including components and general operation.

Source

Sound was generated by a 120 watt, 300 Hz to 6 kHz driver. In the experiment reported herein, the sine wave generator provides a 1560 Hz

$$\left(\omega = \frac{h^* f^*}{c_0^*} = 0.172\right)$$

signal to the amplifier which in turn drives the speaker shown in Fig. 1. The duct temperature was at 27° centigrade. Since the first nonplane mode begins propagating at a frequency of 1701 Hz, the choice of 1560 Hz for the driving frequency guarantees that only plane waves will propagate in the straight portion of the duct far from the area variation.

Test Section

The sound travels through a 10 cm by 3.81 cm (4 in. by 1.5 in.) rectangular test section. This 1.4 meter (56 in.) long section consists of 16 flat detachable plates (8 on top and 8 on the bottom). The variable area test piece, to be described shortly, was inserted in place of the bottom piece at location 6. An exponential horn was attached to the upstream end of the test section. For these experiments, the horn was fitted with an acoustic foam wedge to approximate a $\rho_0 c_0$ termination, which simulates an infinitely long duct.

Variable Area Test Piece

The variable area test piece shown in Fig. 2 was constructed from wood. The surface profile is prescribed by a fourth degree polynominal of the form:

$$Y = \frac{Y^*}{H^*} = 16\left(\frac{x^*}{L^*}\right)^2 - 32\left(\frac{x^*}{L^*}\right)^3 + 16\left(\frac{x^*}{L^*}\right)^4 \qquad (1)$$

where the length L^* is 7.62 cm (3 in.) with a height H^* of 1.91 cm (0.75 in.) which is just half the height of the duct. This curve has zero slope at x^*/L^* equals 0, .5 and 1, and has a maximum slope of 0.77 at x^*/L^* equals 0.21 and 0.79. The symbols used here are defined in the list of symbols.

This test piece has provision for measuring the pressure along the curved surface at x^*/L^* equals 0., 0.3, 0.5, 0.7, and 1.0. The microphone holes at x^*/L^* equals 0.3 and 0.7 correspond with the position of the peak component of the transverse pressure profile, as displayed in Fig. 5 of Ref. 12. The holes were stopped with wooden plugs when the microphones were not in place.

Microphone Installation

Two 0.64 centimeter (1/4 in.) diameter condenser microphones were used to determine the acoustic field. The microphone designated A was used to monitor the source strength of the signal while microphone B was used to determine the pressure and phase angle along both the variable area test piece and along the flat surface above the variable area test piece. The output of each microphone was analyzed to give the rms (root-mean-squared) pressure and phase angle. The flat microphone test holder plate is shown in Fig. 3. This holder is mounted above the variable area test piece in location 6 of Fig. 1. This aluminum plate was fabricated with 0.64 cm (1/4 in.) diameter holes which allowed one microphone (b) to be traversed in the axial direction in increments of 0.953 cm (3/8 in.). The test piece was fabricated with an insulator in each hole, so that the microphones were electrically insulated from the test plate. During a measurement, each microphone's membrane was positioned flush with the surface of the test plate (protective shields were removed).

The response of these microphones was flat to 25 kilohertz. A standard acoustic source was used to check the system amplification. This source generated a 114 decibel signal in 5 octave steps

from 0.125 to 2.0 kilohertz. The microphone was placed in the source and the resulting decibel level of the output was noted. In this way an absolute scale was established for the SPL. In this experiment, the SPL level was set at 100 dB at a position 0.953 cm (3/8 in.) in front of the start of the variable area cross section. The microphone used to monitor the source has been designated as microphone A.

General Procedure

The equipment shown in Fig. 1 was turned on approximately four hours before data were taken. The rms pressure and phase angle were then determined by microphone B in sequence at each axial location along both the flat and curved surfaces. Three measurements were averaged to determine a data set. As a further check on the repeatability of the measurements, a second set of measurements was recorded (data set II). The data is displayed in Tables I and II.

Finally, the data in Table I have been arbitrarily normalized to an average value of 1.4. This is convenient for comparison with the analysis of Ref. 11.

Theory

In this section, a brief review will be presented of a "steady" state finite element theory and a transient finite difference theory. In the following section of this report, these theories will be compared to the experimental data.

Finite Element Theory

For the case of a sheared mean flow in a rectangular duct, Astley and Eversman[11] have developed a finite element method based on weighted residuals using an eight node isoparametric element, shown in Fig. 4.

The acoustic equations are described by the linearized perturbed energy and momentum equations for isentropic flow. The perturbed quantities are assumed to vary with time as $e^{i\omega^* t^*}$, and the theory thereby is called "steady" state theory. Velocities and pressures are nondimensionalized using reference scales, c_0^* and $\rho_0^* c_0^{*2}$, respectively. The following equations result:

$$(x\text{-mom.})\ iku + U_0 \frac{\partial u}{\partial x} + V_0 \frac{\partial u}{\partial y} + u \frac{\partial U_0}{\partial x} + v \frac{\partial U_0}{\partial y} + \frac{1}{\rho_0} \frac{\partial p}{\partial x} - \frac{1}{\gamma p_0 \rho_0} \frac{\partial p_0}{\partial x} p = 0 \qquad (2)$$

$$(y\text{-mom.})\ iku + U_0 \frac{\partial v}{\partial x} + V_0 \frac{\partial v}{\partial y} + u \frac{\partial V_0}{\partial x} + v \frac{\partial V_0}{\partial y} + \frac{1}{\rho_0} \frac{\rho}{y} - \frac{1}{\gamma p_0 \rho_0} \frac{\partial p_0}{\partial y} p = 0 \qquad (3)$$

$$(energy)\ ikp + U_0 \frac{\partial p}{\partial x} + V_0 \frac{\partial p}{\partial y} + u \frac{\partial p_0}{\partial x} + v \frac{\partial p_0}{\partial y} + \gamma \left[\rho_0 \frac{\partial u}{\partial x} + \rho_0 \frac{\partial v}{\partial y} + \rho \frac{\partial U_0}{\partial x} + \rho \frac{\partial V_0}{\partial y} \right] = 0 \qquad (4)$$

The complete details for transforming these equations into the finite element formulation can be found in Ref. 11.

The speaker, see Fig. 1, sends acoustic pressure waves into the duct which are either reflected or transmitted by the variable area duct restriction. Accurate source modelling and representation of the duct termination requires special consideration. Acoustic mode reflection at the inlet to the duct nonuniformity and the transmission without reflection at the outlet of the nonuniformity is modelled by matching the finite element solution in the interior of the nonuniformity to analytical or finite element eigen function expansions in the uniform inlet and outlet ducts. This permits a multimodal representation accounting for reflection and mode conversion by the nonuniformity. This approach was first introduced in the acoustic problem by Eversman, Cook and Beckemeyer[14] in connection with a modified Galerkin solution for transmission in nonuniform ducts without flow and was subsequently used in a similar context in the presence of flow[11,15].

The boundary condition at the upper and lower hard walls requires that the normal acoustic velocity be zero.

Transient Finite Difference Theory

White[12] has numerically mapped the variable area duct into the rectangular geometry shown in Fig. 5. The wave equation in the physical xy plane

$$\omega^2 P_{tt} = P_{xx} + P_{yy} \qquad (5)$$

was transformed to the ξ,η plane

$$\omega^2 P_{tt} = \frac{1}{J^2} \left[\alpha P_{\xi\xi} - 2\beta P_{\xi\eta} + \gamma_1 P_{\eta\eta} + \sigma P_{\eta} + \tau P_{\xi} \right] \qquad (6)$$

where $J, \alpha, \beta, \gamma_1, \sigma$ and τ are functions of x, y, z and η and are defined in Ref. 12. The mapping from the physical to the transformed ξ,η plane was performed numerically using a technique developed by Thompson (Refs. 16 and 17). Equation (6) was then rewritten in finite difference form and solved.

The entrance and exit conditions used in the transient finite difference theory were

$$\frac{P(o,y,t)}{e^{i\omega^* t^*}} = 1 \qquad (7)$$

and an exit impedance value of

$$Z_e^* \Big|_{x/L = 1} = \rho_0^* c_0^* \qquad (8)$$

both Eqs. (7) and (8) represent approximations to the entrance and exit conditions employed by Astley and Eversman (Ref. 11) discussed earlier. At the entrance and exit of the variable area section, higher order acoustic modes will generally yield a non-uniform pressure profile and a non-uniform exit impedance. The degree which Eqs. (7) and (8) approximate the true entrance conditions can be improved by adding both straight entrance and exit sections. In these sections, the higher order modes will decay such that Eqs. (7) and (8) will more closely approximate the true boundary conditions.

Discussion of Results

In this section, experimental results are discussed in the following categories: rms axial pressure profiles, transverse pressure profiles and phase angle.

RMS Axial Pressure Profiles

The normalized rms pressures from Table I are plotted against axial distance in Fig. 6 and compared to the theories of Refs. 11 and 12. As seen in Fig. 6, the Astley-Eversman theory is in excellent agreement with the data. In their analysis, the incident pressure wave had a value of 1; thus, the 1.4 value at $x = 0$ indicates a reflected wave of 0.4 in magnitude.

The White transient finite difference theory shown by the dashed line in Fig. 6 is also in reasonably good agreement with the data. Some deviation of the pressure at x^*/L^* equals 1.0 is seen.

Transverse Pressure Profile

Figure 7 shows a comparison between the measured and calculated transverse pressure profiles. Both theories predict very small differences in pressure between the flat ($y = 0$) and the curved surface ($y = 1$). The scatter in the data appear large because the profile is nearly flat; thus the pressure differences in Fig. 6 are very small. Also, the pressure at $x = 0.3$ on the flat surface had to be estimated from Fig. 6 because a microphone was not at this exact location on the flat surface. Nevertheless, both theories predict the proper trends of the data and are in reasonable agreement in magnitude with the test data.

Phase Angle

Figure 8 shows a comparison between the measured and calculated value of the phase angle as a function of axial distance. Again both theories are in reasonable agreement with the data. In this case, the transient finite difference theory gives slightly better agreement at x^*/L^* of 1. Overall, considering Figs. 7 and 8, both theories appear to perform equally well in correlating the data.

Standing Wave Pattern

The duct construction in the present experiment produced a reflection which induced a significant standing wave pattern ahead of the test section. Also, any reflection from the duct termination will generate standing waves downstream of the test section. To determine this wave pattern, rms pressure measurements were taken along the flat wall both upstream and downstream of the test section. These measurements are recorded in Table III and plotted in Fig. 9. As seen in Fig. 9, the finite element theory and the transient finite difference theory are in excellent agreement with the data upstream of the test section. Since the theory assumes that there is no reflected energy at the exit, a downstream standing wave pattern cannot, of course, arise.

The standing wave ratio S downstream of the test section was

$$S = \frac{0.905}{0.83} = 1.09 \tag{9}$$

Therefore, assuming the incident and reflected waves react in normal incidence at the duct exit, the sound power reflection coefficient is (Ref. 18, p. 301)

$$\alpha_r = \left(\frac{S - 1}{S + 1}\right)^2 = 0.00185 \tag{10}$$

This slight amount of reflected sound from the duct exit probably accounts for part of the deviation between experiment and theory which assumes a non-reflecting exit termination.

With the exception of the Astley-Eversman modal coupling finite element formulation, all other numerical analyses specify an entrance pressure or velocity and an approximate exit impedance. White's analysis, which uses Eqs. (7) and (8) for the entrance and exit conditions, is typical of these theories. Direct prediction of the transmitted and reflected energy is not generally possible in these theories. For low frequency plane wave propagation (Ref. 18, p. 300, Ref. 19), however, an estimate of the reflection coefficient can be found by adding a straight section of duct ahead of the area variations and measuring the standing wave pattern in the region where higher order modes have decayed. Higher order modes will be generated at the interface between the straight and variable area portion of the duct.

In contrast, the Astley-Eversman finite element formulation predicts the transmitted and reflected energy by analytical including a straight entrance and exit section; therefore, their analysis does not require elements in these sections. Application of the Astley-Eversman theory to only the contracting portion of the duct yielded a reflection coefficient of 0.264. This coefficient can now be compared to the reflection coefficient obtained from the measured and predicted standing wave pattern shown in Fig. 9.

From Fig. 9, the standing wave ratio is

$$S = \frac{1.52}{0.49} = 3.120 \tag{11}$$

Since only plane waves propagate in the straight portion of the duct at $\omega = 0.172$, the power reflection coefficient can be calculated directly (Ref. 18, Eq. 8.49).

$$\alpha_r = \frac{(3.102 - 1)^2}{(3.102 + 1)^2} = 0.263 \tag{12}$$

which is in excellent agreement with the value predicted by the Astley-Eversman modal coupling theory. Therefore, in a general situation where it is desired to estimate the reflected or transmitted acoustic energy, the eigenvalue formulation of Astley and Eversman for the duct entrance and exit condition would be the appropriate algorithm to use. There could be some difficulty, however, in estimating the modal content of the incident wave if higher order modes can propagate.

Conclusion

Experimental data have been presented for sound propagation in a simulated infinite hard wall duct with a large change in duct cross sectional area. The data is conveniently tabulated for further use. The "steady" state finite element theory of Astley and Eversman and the transient finite difference theory of White are in good agreement with the data for both the axial and transverse pressure profiles and the axial phase angle. Therefore, numerical finite difference and finite element theories appear to be ideally suited for handling duct propagation problems which encounter large axial gradients in acoustic parameters.

The measured energy reflection coefficient agrees with the values from the Astley-Eversman modal coupling model. Therefore, in a general multi-modal situation where it is desired to estimate the reflected or transmitted acoustic energy, the eigenvalue formulation of Astley and Eversman for the duct entrance and exit conditions would be the approximate algorithm to use. Definition of the mode content of the incident wave might represent a problem, however.

References

1. Baumeister, K. J., "Numerical Techniques in Linear Duct Acoustics - A Status Report," ASME Paper 80-WA/NC-2, Nov. 1980. (NASA TM-81553).

2. Plumblee, H. E., "A Theoretical and Experimental Study of Sound Attenuation in an Annular Duct," AIAA Paper 73-1005, Oct. 1973.

3. Plumblee, H. E., Dean, P. D., Wynne, G. A., and Burrin, R. H., "Sound Propagation in and Radiation from Acoustically Lined Flow Ducts: A Comparison of Experiment and Theory," NASA CR-2306, 1973.

4. Lester, H. C. and Parott, T. L., "Comparison of Measured and Predicted Impedance at Grazing Incidence," AIAA Journal, Vol. 18, No. 5, May 1980, pp. 504-508.

5. Kagawa, Y. and Omote, T., "Finite-Element Simulation of Acoustic Filters of Arbitrary Profile with Circular Cross Section," Journal of the Acoustical Society of America, Vol. 60, No. 5, Nov. 1976, pp. 1003-1013.

6. Kagawa, Y., Yamabuchi, T., and Mori, A., "Finite Element Simulation of an Axisymmetric Acoustic Transmission System with a Sound Absorbing Wall," Journal of Sound and Vibration, Vol. 53, No. 3, 1977, pp. 357-374.

7. Kagawa, Y., Yamabuchi, T., and Yoshikawa, T., "Finite Element Approach to Acoustic Transmission-Radiation Systems and Application to Horn and Silencer Design," Journal of Sound and Vibration, Vol. 69, No. 2, 1980, pp. 207-228.

8. Tag, I. A. and Lumsdaine, E., "An Efficient Finite Element Technique for Sound Propagation in Axisymmetric Hard Wall Ducts Carrying High Subsonic Mach Number Flows," AIAA Paper 78-1154, July 1978.

9. Nayfeh, A. H., Kaiser, J. E., Marshall, R. L., and Hurst, C. J., "An Analytical and Experimental Study of Sound Propagation and Attenuation in Variable-Area Ducts," Virginia Polytechnic Inst. and State Univ., Blacksburg, VA, Oct. 1978. (NASA CR-135392)

10. Nayfeh, A. H., Kaiser, J. E., Marshall, R. L., and Hurst, C. J., "A Comparison of Experiment and Theory for Sound Propagation in Variable Area Ducts," Journal of Sound and Vibration, Vol. 71, July 1980, pp. 241-259.

11. Astley, R. J. and Eversman, W., "Acoustic Transmission in Non-Uniform Ducts with Mean Flow, Part II: The Finite Element Method," Journal of Sound and Vibration, Vol. 74, Jan. 1981, pp. 103-121.

12. White, J. W., "A General Mapping Procedure for Variable Area Duct Acoustics," AIAA Paper 81-0094, Jan. 1981.

13. Succi, G. P., Baumeister, K. J., and Ingard, K. U., "Interaction of a Turbulent Jet Noise Source with Transverse Modes in a Rectangular Duct," NASA TP-1248, 1978.

14. Eversman, W., Cook, E. L., and Beckemeyer, R. J., "A Method of Weighted Residuals for the Investigation of Sound Transmission in Nonuniform Ducts without Flow," Journal of Sound and Vibration, Vol. 38, Jan. 1975, pp. 105-123.

15. Eversman, W. and Astley, R. J., "Acoustic Transmission in Non-Uniform Ducts with Mean Flow, Part I: The Method of Weighted Residuals," Journal of Sound and Vibration, Vol. 74, Jan. 1981, pp. 89-101.

16. Thompson, J. F., Thames, F. C., and Mastin, C. W., "Automatic Numerical Generation of Body-Fitted Curvilinear Coordinate System for Field Containing Any Number of Arbitrary Two-Dimensional Bodies," Journal of Computational Physics, Vol. 15, July 1974, pp. 299-319.

17. Thompson, J. F., Thames, F. C., and Mastin, C. W., "Boundary-Fitted Curvilinear Coordinate Systems for Solution of Partial Differential Equations on Fields Containing Any Number of Arbitrary Two-Dimensional Bodies," NASA CR-2729, 1977.

18. Reynolds, D. D., Engineering Principles of Acoustics, Allyn and Bacon, Inc., Boston, MA, 1981.

19. Cabelli, A., "The Acoustic Characteristics of Duct Bends," Journal of Sound and Vibration, Vol. 68, Feb. 1980, pp. 369-388.

TABLE I. - AXIAL PRESSURE MEASUREMENTS

Straight Wall

MIC ℄ position X*/L*	Data Set I, P_{rms}				Data Set II, P_{rms}			
	1	2	3	Average	1	2	3	Average
0.0	1.395	1.390	1.418	1.40	1.405	1.403	1.395	1.40
.125	1.556	1.473	1.508	1.513	1.443	1.468	1.493	1.468
.250	1.490	1.508	1.488	1.495	1.500	1.480	1.500	1.493
.375	1.397	1.385	1.387	1.390	1.405	1.380	1.400	1.395
.50	1.252	1.234	1.239	1.242	1.214	1.217	1.237	1.222
.625	1.066	1.069	1.046	1.061	1.049	1.066	1.061	1.059
.750	.918	.918	.916	.918	.941	.933	.941	.938
.875	.835	.841	.868	.848	.851	.851	.863	.856
1.0	.810	.825	.825	.820	.805	.815	.823	.815

Curved Wall

MIC ℄ position X*/L*	Data Set I, P_{rms}				Data Set II, P_{rms}			
	1	2	3	Average	1	2	3	Average
-0.125	1.405	1.443	1.440	1.43	1.387	1.382	1.423	1.397
.3	1.573	1.535	1.578	1.536	1.490	1.553	1.551	1.530
.5	1.259	1.254	1.227	1.247	1.219	1.239	1.295	1.219
.7	.956	.938	1.006	.966	.936	.911	.951	.933
1.125	.876	.883	.886	.881	.848	.863	.891	.868

TABLE II. - PHASE ANGLE DATA

Straight Wall

MIC ℄ position X*/L*	Data Set I, ϕ				Data Set II, ϕ			
	1	2	3	Average	1	2	3	Average
0.0	0.	0.	0.	0.	0.	0.	0.	0.
.125	5.70	6.5	6.2	6.13	6.1	6.3	6.2	6.2
.250	12.6	13.0	12.9	12.83	13.0	13.0	13.0	13.0
.375	21.2	22.0	21.3	21.5	21.4	21.4	21.4	21.4
.50	32.4	33.3	32.8	32.83	32.8	32.8	32.9	32.83
.625	47.9	48.6	48.4	48.3	48.1	48.1	48.3	48.17
.750	66.0	66.6	66.6	66.4	66.6	66.7	66.7	66.67
.875	86.4	86.9	86.1	86.47	86.4	86.5	86.5	86.47
1.0	105.6	106.6	106.8	106.33	106.4	106.4	106.4	106.4

Curved Wall

MIC ℄ position X*/L*	Data Set I, ϕ				Data Set II, ϕ			
	1	2	3	Average	1	2	3	Average
-0.125	-4.47	-4.27	-4.87	-4.54	-5.10	-5.30	-5.0	-5.13
.3	10.43	10.93	10.43	10.6	10.1	10.6	10.1	10.27
.5	32.83	32.63	32.43	32.63	32.3	32.5	32.3	32.37
.7	71.23	72.13	72.73	72.03	71.7	71.4	71.5	71.53
1.125	119.73	119.83	120.13	119.9	119.2	119.5	119.4	119.37

TABLE III. – STANDING WAVE DATA

X*/L*	P_{rms}	ϕ	X*/L*	P_{rms}	ϕ
0.	1.4	0.	0.	1.40	0.
-.125	1.252	-7.2	.125	1.493	6.5
-.250	1.009	-16.7	.250	1.474	13.5
-.583	.491	-92.7	.375	1.383	22.3
-.605	.508	-99.8	.5	1.238	33.8
-.730	.711	-133.2	.625	1.071	49.1
-.855	.987	-150.0	.750	.939	67.2
-.980	1.217	-159.6	.875	.868	86.5
-1.083	1.386	-165.4	1.0	.824	105.5
-1.105	1.392	-166.3	1.125	.804	124.1
-1.208	1.512	-171.0	1.250	.804	141.9
-1.230	1.484	-171.9	1.375	.816	159.3
-1.333	1.512	-176.4	1.50	.841	176.1
-1.355	1.491	-176.8	1.625	.865	-168.6
-1.458	1.428	178.2	1.958	.902	-129.7
-1.480	1.415	177.5	2.083	.907	-115.2
-1.583	1.274	171.6	2.208	.907	-100.6
-1.605	1.263	170.6	2.333	.873	-85.5
-1.708	1.033	162.2	2.458	.858	-70.1
-1.730	1.002	160.6	2.583	.843	-53.9
-1.833	.769	146.9	2.708	.829	-37.4
-1.855	.727	143.7	2.833	.831	-20.7
-1.98	.531	110.2	2.958	.841	-4.3
-2.105	.564	67.5	3.083	.868	11.2
-2.23	.822	40.5	3.208	.885	26.3
-2.355	1.039	26.5	3.333	.902	40.8
-2.48	1.330	18.3	3.458	.905	54.8
			3.583	.888	69.2
			3.708	.880	84.1
			3.833	.846	99.2

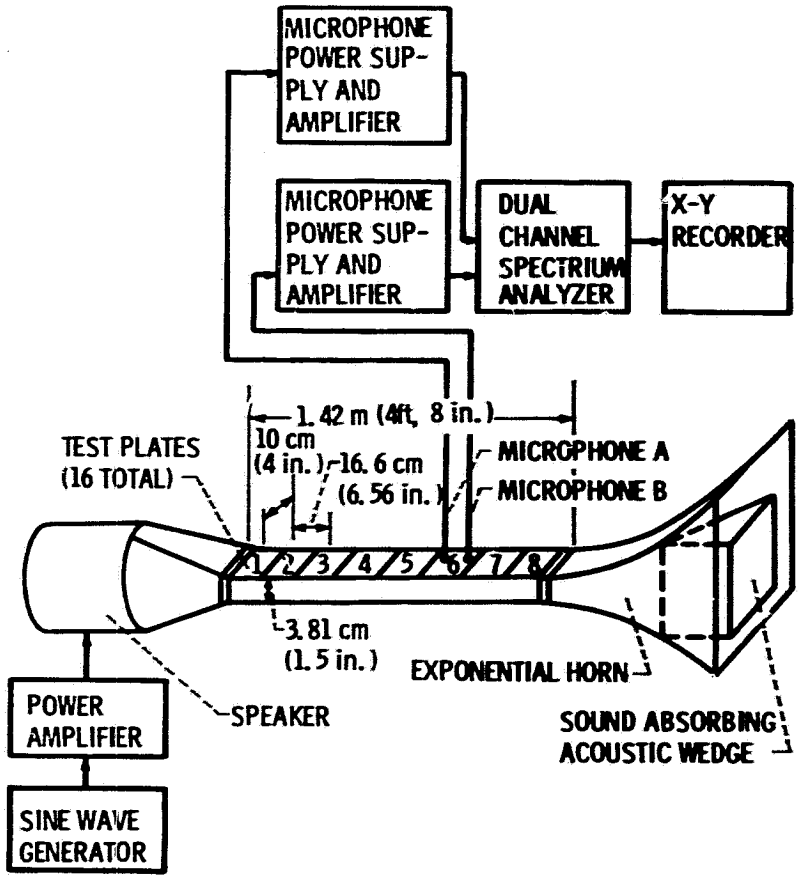

Figure 1. – No flow acoustic duct test section and instrumentation.

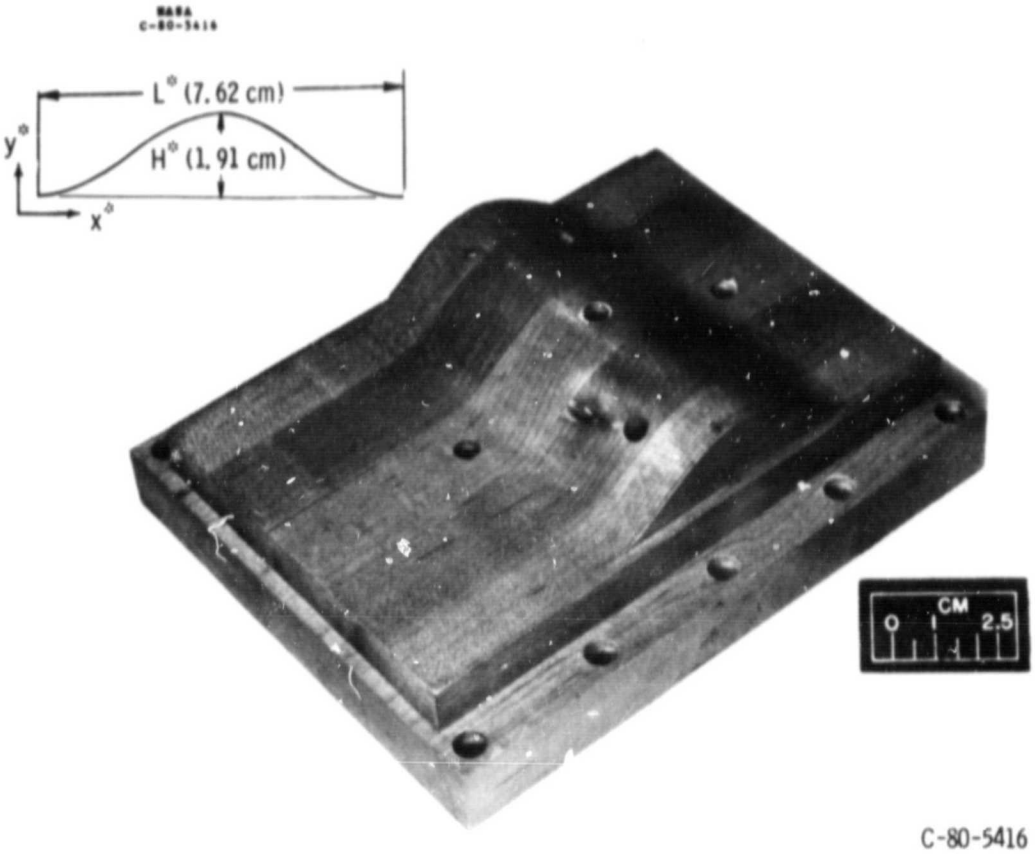

Figure 2. - Variable area test piece with 5 microphone locations (microphone plugs not shown).

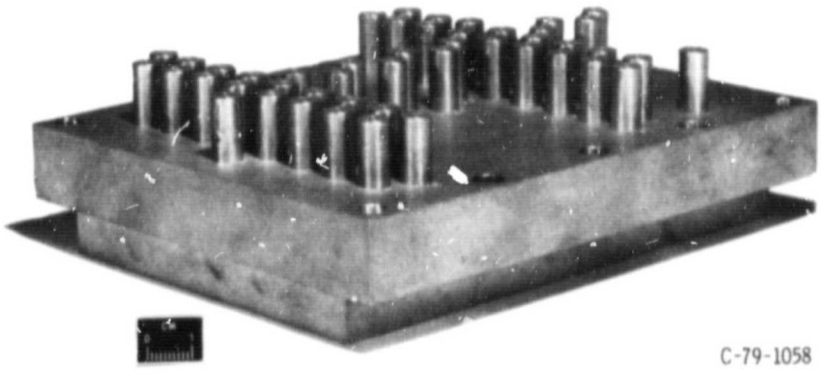

Figure 3. - Microphone test holder plate mounted above the variable area test piece.

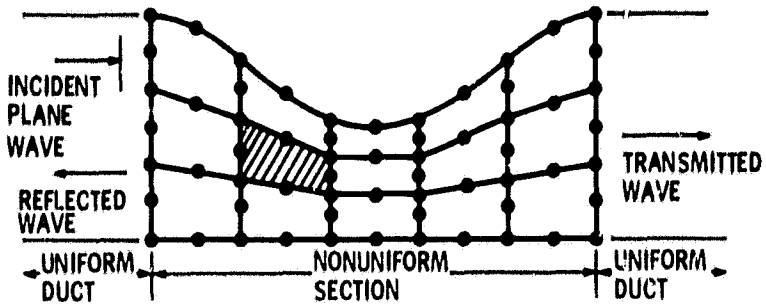

Figure 4. - Finite element discretization of variable area duct using theory of reference 11.

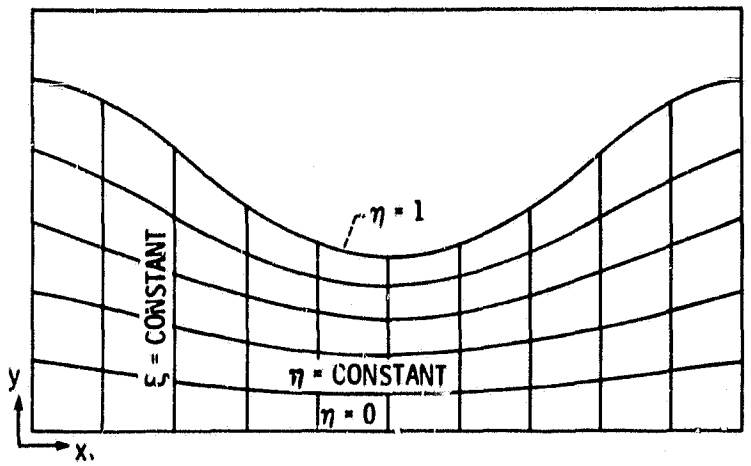

(a) REAL PLANE.

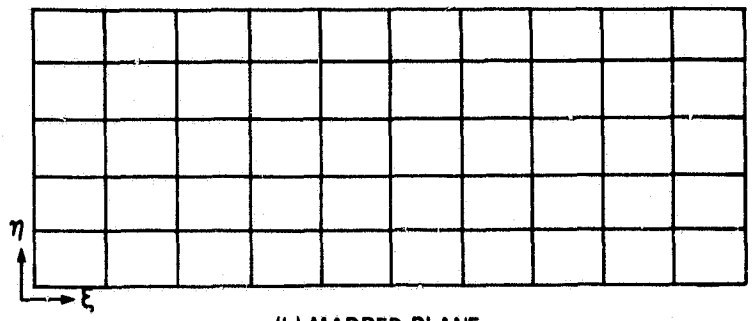

(b) MAPPED PLANE.

Figure 5. - Mapping for a variable area duct.

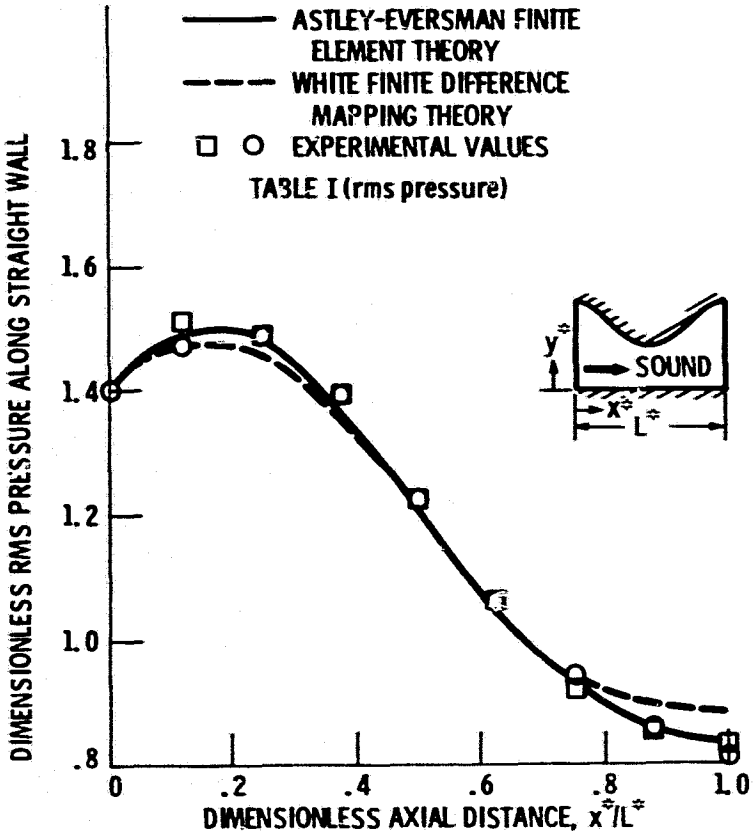

Figure 6. – Experimental and theoretical axial pressure profiles (ω = 0.172).

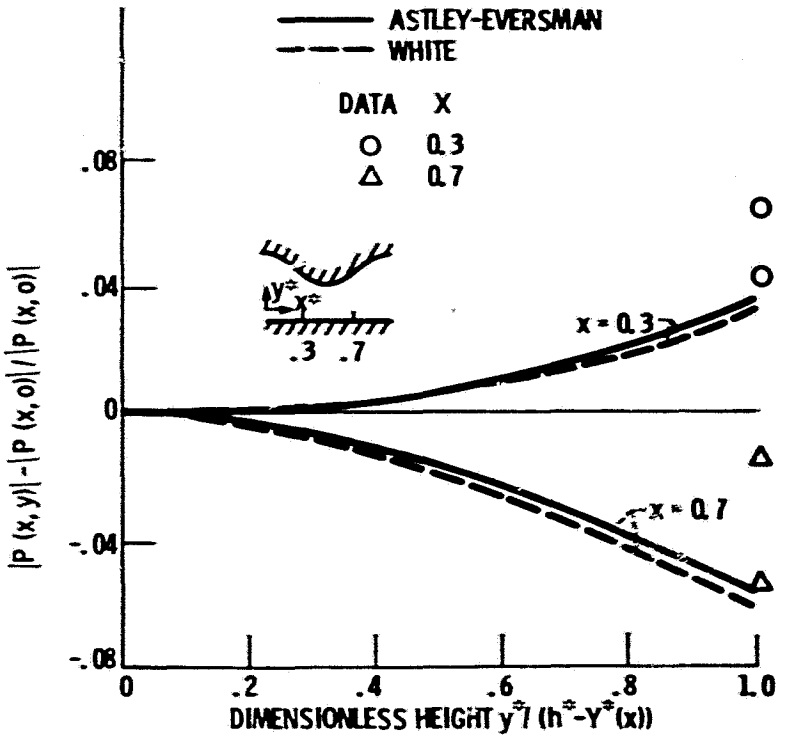

Figure 7. – Experimental verification of trends in transverse pressure profiles.

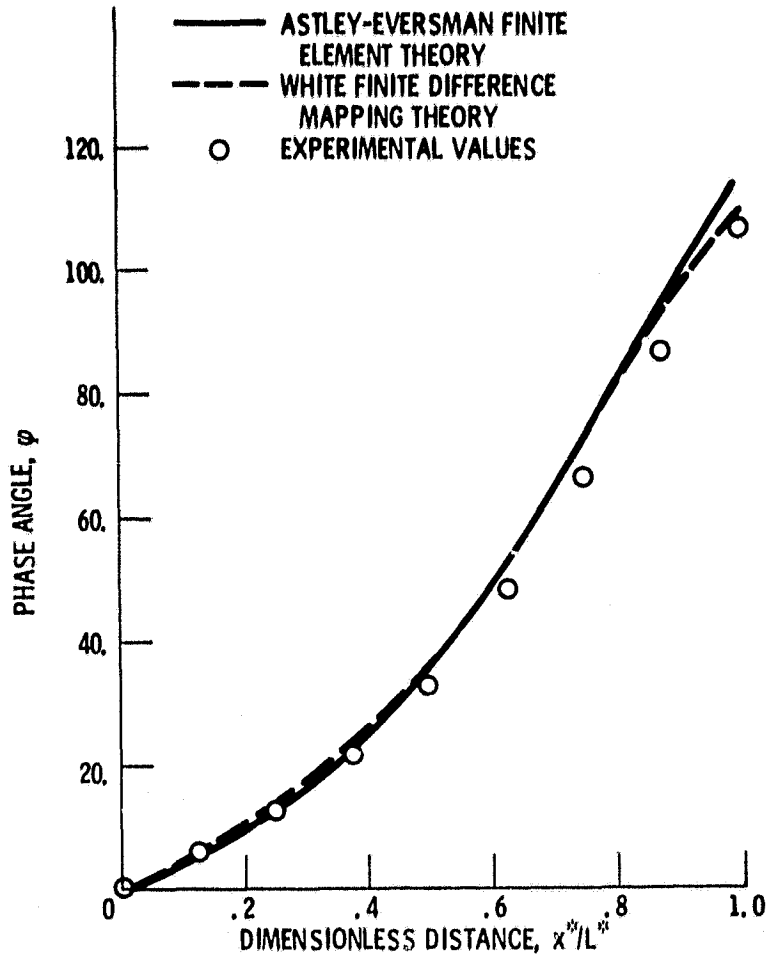

Figure 8. - Experimental and theoretical axial phase angles (w = 0.172).

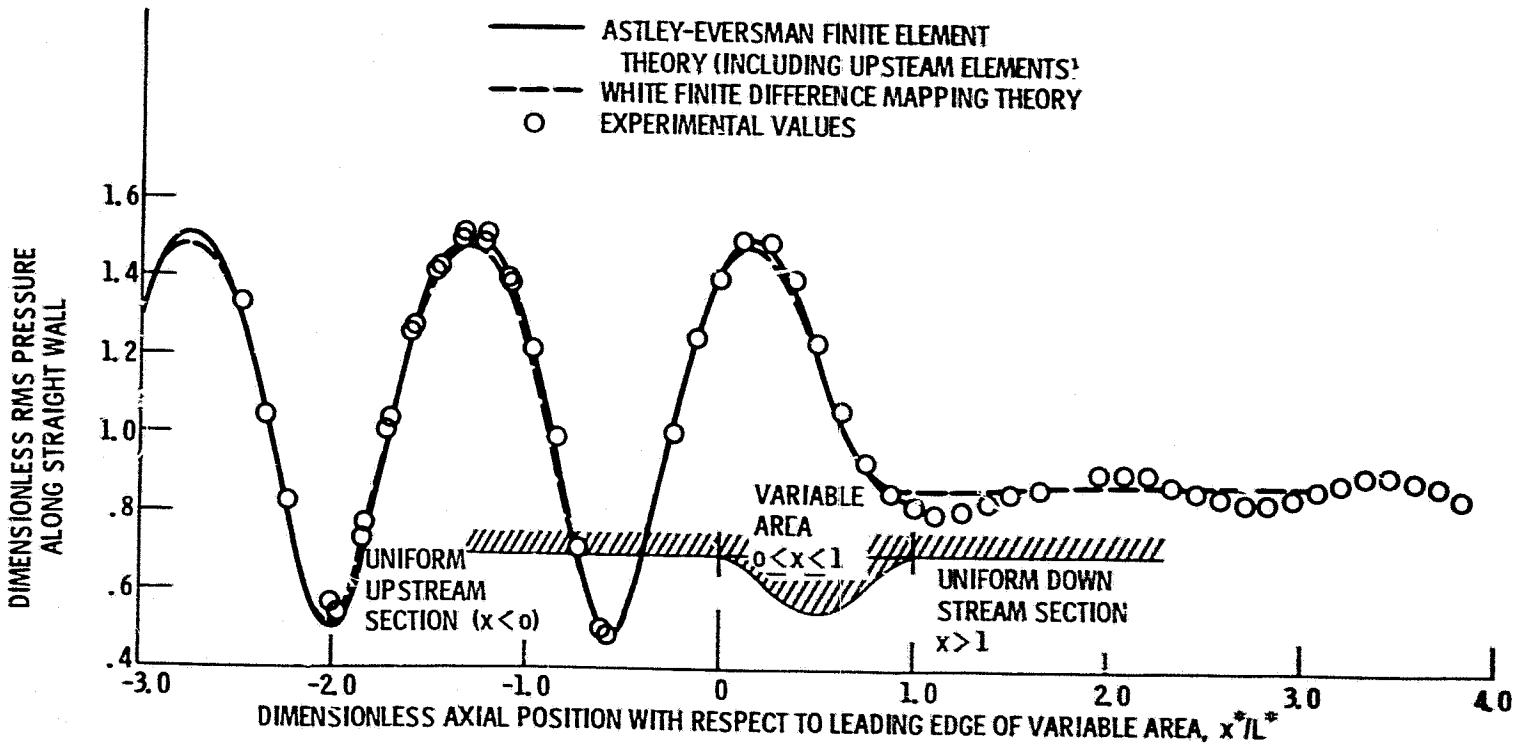

Figure 9. - Experimental and theoretical axial standing wave pressure profiles.